DOT/FAA/CT-82/61

Numerical Calculations of Turbulent Buoyant Flow in Aircraft Cabins

K.T. Yang
J.R. Loyd
A.M. Kanury
K. Satoh

March 1983

Final Report

US Department of Transportation
Federal Aviation Administration
Technical Center
Atlantic City Airport, N.J. 08405

US 8351 8w
~~US 375~~ 1

BIBLIOGRAPHIC DATA SHEET	1. Report No. DOT/FAA/CT-82/61	2.	3. Recipient's Accession No.

4. Title and Subtitle

Numerical Calculations of Turbulent Buoyant Flow in Aircraft Cabins

5. Report Date
March 1983

6.

7. Author(s)
K.T. Yang, J.R. Lloyd, A.M. Kanury and K. Satoh

8. Performing Organization Rept. No.

9. Performing Organization Name and Address
Fire Research Group
Department of Aerospace and Mechanical Engineering
University of Notre Dame
Notre Dame, IN 46556

10. Project/Task/Work Unit No.

11. Contract/Grant No.
NBS NB81 NADA 2000

12. Sponsoring Organization Name and Address
U. S. Department of Transportation
Federal Aviation Administration Technical Center
Atlantic City, New Jersey 08405

13. Type of Report & Period Covered
Technical Report

14.

15. Supplementary Notes

16. Abstracts

The UNDSAFE computer code is utilized to study the spread of fire and smoke in aircraft cabins due to fires located in the cabin floor. A simulation study is first made based on expected data to establish the equivalence between two-dimensional and three-dimensional parameters including fire distribution and shape, the doorway height, and level of turbulence and also the effects of these parameters on the fire and smoke spread. The computer code is then used to simulate the spread of fire and smoke in a wide-body aircraft cabin with and without seats for two different scenarios of the fire location. The results show the dramatic effects of the seats on the flow, temperature, and smoke concentration behaviors inside the cabin. Important parameters have been identified such as the seat back height and the configuration of the seat bottom, closed or open.

17. Key Words and Document Analysis. 17a. Descriptors

Fire
Smoke
Aircraft
Turbulence
Buoyancy
Numerical
Finite Difference
Flame
Vent

17b. Identifiers/Open-Ended Terms

UNDSAFE

17c. COSATI Field/Group FIRE RESEARCH

18. Availability Statement	19. Security Class (This Report)	21. No. of Pages
RELEASED UNLIMITED	UNCLASSIFIED	43
	20. Security Class (This Page) UNCLASSIFIED	22. Price

INSTRUCTIONS FOR COMPLETING FORM NTIS-35

(Bibliographic Data Sheet based on COSATI Guidelines to Format Standards for Scientific and Technical Reports Prepared by or for the Federal Government, PB-180 600).

1. **Report Number.** Each individually bound report shall carry a unique alphanumeric designation selected by the performing organization or provided by the sponsoring organization. Use uppercase letters and Arabic numerals only. Examples FASEB-NS-73-87 and FAA-RD-73-09.

2. Leave blank.

3. **Recipient's Accession Number.** Reserved for use by each report recipient.

4. **Title and Subtitle.** Title should indicate clearly and briefly the subject coverage of the report, subordinate subtitle to the main title. When a report is prepared in more than one volume, repeat the primary title, add volume number and include subtitle for the specific volume.

5. **Report Date.** Each report shall carry a date indicating at least month and year. Indicate the basis on which it was selected (e.g., date of issue, date of approval, date of preparation, date published).

6. **Performing Organization Code.** Leave blank.

7. **Author(s).** Give name(s) in conventional order (e.g., John R. Doe, or J.Robert Doe). List author's affiliation if it differs from the performing organization.

8. **Performing Organization Report Number.** Insert if performing organization wishes to assign this number.

9. **Performing Organization Name and Mailing Address.** Give name, street, city, state, and zip code. List no more than two levels of an organizational hierarchy. Display the name of the organization exactly as it should appear in Government indexes such as Government Reports Index (GRI).

10. **Project/Task/Work Unit Number.** Use the project, task and work unit numbers under which the report was prepared.

11. **Contract/Grant Number.** Insert contract or grant number under which report was prepared.

12. **Sponsoring Agency Name and Mailing Address.** Include zip code. Cite main sponsors.

13. **Type of Report and Period Covered.** State interim, final, etc., and, if applicable, inclusive dates.

14. **Sponsoring Agency Code.** Leave blank.

15. **Supplementary Notes.** Enter information not included elsewhere but useful, such as: Prepared in cooperation with . . . Translation of . . . Presented at conference of . . . To be published in . . . Supersedes . . . Supplements . . . Cite availability of related parts, volumes, phases, etc. with report number.

16. **Abstract.** Include a brief (200 words or less) factual summary of the most significant information contained in the report. If the report contains a significant bibliography or literature survey, mention it here.

17. **Key Words and Document Analysis. (a). Descriptors.** Select from the Thesaurus of Engineering and Scientific Terms the proper authorized terms that identify the major concept of the research and are sufficiently specific and precise to be used as index entries for cataloging.
(b). Identifiers and Open-Ended Terms. Use identifiers for project names, code names, equipment designators, etc. Use open-ended terms written in descriptor form for those subjects for which no descriptor exists.
(c). COSATI Field/Group. Field and Group assignments are to be taken from the 1964 COSATI Subject Category List. Since the majority of documents are multidisciplinary in nature, the primary Field/Group assignment(s) will be the specific discipline, area of human endeavor, or type of physical object. The application(s) will be cross-referenced with secondary Field/Group assignments that will follow the primary posting(s).

18. **Distribution Statement.** Denote public releasability, for example "Release unlimited", or limitation for reasons other than security. Cite any availability to the public, other than NTIS, with address, order number and price, if known.

19 & 20. **Security Classification.** Do not submit classified reports to the National Technical Information Service.

21. **Number of Pages.** Insert the total number of pages, including introductory pages, but excluding distribution list, if any.

22. **NTIS Price.** Leave blank.

PREFACE

This work was sponsored by the National Bureau of Standards, Center for Fire Research, through an interagency agreement with the Federal Aviation Administration. The Technical Monitor was Dr. Walter Jones. The valuable advice and encouragement during the course of this work from Dr. Thor I. Eklund of the FAA Technical Center, Drs. James Quintiere and Walter Jones of the NBS Center for Fire Research are sincerely appreciated.

TABLE OF CONTENTS

LIST OF ILLUSTRATIONS

LIST OF ILLUSTRATIONS

LIST OF SYMBOLS

A	coefficients
C_p	specific heat
D	diffusion coefficient
g	gravitational acceleration
H	height of aircraft cabin
K	constant
k	thermal conductivity
ℓ	mixing length
P	pressure
P_r	Prandtl number
R	gas constant
R_e	Reynolds number
R_i	gradient Richardson number
S	volumetric function
S_c	Schmidt number
T	temperature
t	time variable
U_o	reference velocity
u,v	velocity components
x,y	coordinates
Y	smoke concentration
$\Delta x,\Delta y,\Delta t$	dimensionless step sizes
μ	viscosity
ρ	density
τ	shear stress

Superscript

-	dimensionless quantities

Subscripts

E	hydrostatic equilibrium conditions
eff	effective (laminar plus turbulent)
o	reference quantities
P	calculation cell
S,W,E,N	neighboring cells
tb	turbulent

EXECUTIVE SUMMARY

The majority of prior efforts to mathematically model aircraft fires with computer codes have employed zone models. In the simpler zone models, the products of combustion of a fire in the cabin flow to a hot zone near the ceiling. In this zone, temperature is considered to be uniform both in the vertical and horizontal directions. Below this hot zone is a cool zone which is also considered uniform in temperature.

Because experimental fire data show gradients in the hot zone in the longitudinal direction along the fuselage centerline, an effort to predict the details of this temperature distribution was undertaken with a differential field model computer code. In the field model, the partial differential equations governing fluid flow are solved over a specified grid network. In this fashion, more details of temperature and fluid velocity are available within the hot and cool zones. The code used in this effort is known by the acronym UNDSAFE (University of Notre Dame Smoke and Fire in Enclosures).

The primary findings of this effort are as follows:

1. The strength of the fire source affects only the temperature level in the upper parts of the cabin, while the lengthwise temperature variations remain essentially unaffected.

2. The two-dimensional field model could successfully predict cabin thermal profiles generated by pan fires in tests conducted at the Johnson Space Center.

3. Given fire sources in the vicinity of seats, the model showed significant changes in the flows of the products of combustion depending on seat back height and seat clearances from the floor.

INTRODUCTION

PURPOSE

The overall purpose of this study is to simulate aircraft cabin fire pheomena by means of a differential field model computer code for the purpose of better understanding the dynamics of fire and smoke spread in aircraft cabins. The basic code is known by the acronym UNDSAFE (University of Notre Dame Smoke and Fire in Enclosures).

BACKGROUND

In survivable aircraft accidents involving fires, there is a great need to understand the flow behavior of heat and toxic gases in the cabin. There are two basic types of fire scenarios in such accidents. The first type is in the presence of a fuselage break or door opening when fire is initiated outside the cabin due to burning of the spilled fuel. In this case the movement of fire and toxic gases into the cabin may be influenced by heat radiation through the fuselage opening and by convection due to the prevailing wind close to the ground. The fire spread into the cabin will be affected by the location of the fire, ground wind direction and speed, and the geometry of the opening. On the other hand, the effect of direct radiant heating depends primarily on the flame temperature, geometry of the opening, and the cabin material. The second fire scenario deals with fire spread inside the aircraft cabin, which may be due to either the hot gases from the external fire coming through the opening, or to a fire initiated inside the cabin. The latter type situation might occur during flight. The spread of fire and hot toxic gases resulting from propagation of the combustion process within the cabin interior depends on the cabin material contents, interior cabin partitioning, fuselage openings, and arrangements of seat rows. These two scenarios are deemed to be of critical importance to the Federal Aviation Administration (FAA) in dealing with the overall problem of fire safety. The development of valid predictive schemes for these scenarios can provide inputs to the eventual development for fire-safety countermeasures. The second of the above-mentioned scenarios is the subject of a recent numerical study based on the application of the UNDSAFE computer code developed originally for turbulent bouyant flows simulating a fire due to a volumetric heat source in a two-dimensional compartment with venting,[1,2] with modifications to include the effects of one-dimensional ceiling-floor radiation[3]. The purpose of this report is to present the results of this study.

In the following sections, the validity of the numerical model is first demonstrated by comparing the calculated results with a set of experimental data from cabin mockup fire tests conducted at the Johnson Space Center. This is then followed by the presentation of the results of computer simulation runs to determine the effects of the location of the fire source, seating arrangements, and venting in a designated aircraft cabin on the spread of fire and smoke within the cabin.

COMPUTER MODEL VALIDATION

CHOICE OF EXPERIMENTAL DATA FOR MODEL VALIDATION

A series of cabin mockup fire tests[4] was conducted at the Johnson Space Center to produce test data for the verification of the DACFIR (Dayton Aircraft Cabin Fire) zone model developed at the (University of Dayton Research Institute) (UDRI) under FAA sponsorship.[5] The test cabin geometry is shown in Figure 1. Instantaneous temperature distributions in both longitudinal and vertical directions were measured and recorded for each test run. The design and conduct of the test has been formally reported by the National Aeronautics and Space Administration[4]. In view of certain missing details of the test runs, it was decided, after consultation with FAA, UDRI and the Center for Fire Research at the National Bureau of Standards, that test 3-B provided the best suitable experimental data for validation of the numerical computations. While the UNDSAFE computer code, modified for the aircraft cabin geometry shown in Figure 1, is fully capable of handling ceiling heat losses and unsteady fuel weight-loss rates at the burner, the experimental temperature distributions at the 60-second point from the initiation of the fire were specifically chosen for comparison with the numerical results. At such a time instant, the ceiling heat loss can still be neglected and the fuel weight loss rate can be taken to be a constant. And yet, the computations at this time instant are already far away from the initial conditions so that the effect of the initial ramping of the heat source required in the numerical scheme has essentially vanished. This simplification thus enabled us to concentrate on the simulation of more important parameters such as the heat load, the fire size, the doorway height, and the level of turbulence in the test cabin. The corresponding measured temperature distributions at this time instant are shown in Figure 2. Note the the constant fuel weight loss rate in this case corresponds to an energy input into the cabin of approximately 235 KW based on the heating value of the fuel. These temperatures form the basis for comparison with the results of the numerical computations.

DIFFERENTIAL FIELD MODEL FOR THE UNDSAFE COMPUTER CODE

The simulated two-dimensional geometry of the aircraft cabin in Figure 1 is shown in Figure 3. The UNDSAFE code is based on a primitive-variable differential-field model which takes into account strong buoyancy, turbulence, and compressibility. Details are already given in references 1, 3, and 6, hence only a brief outline will be presented herein. For two-dimensional turbulent buoyant flow in a rectangular enclosure, such as that in Figure 3, the governing conservation differential equation in the physical primitive variables are well known and may be non-dimensionalized by introducing the following definitions:

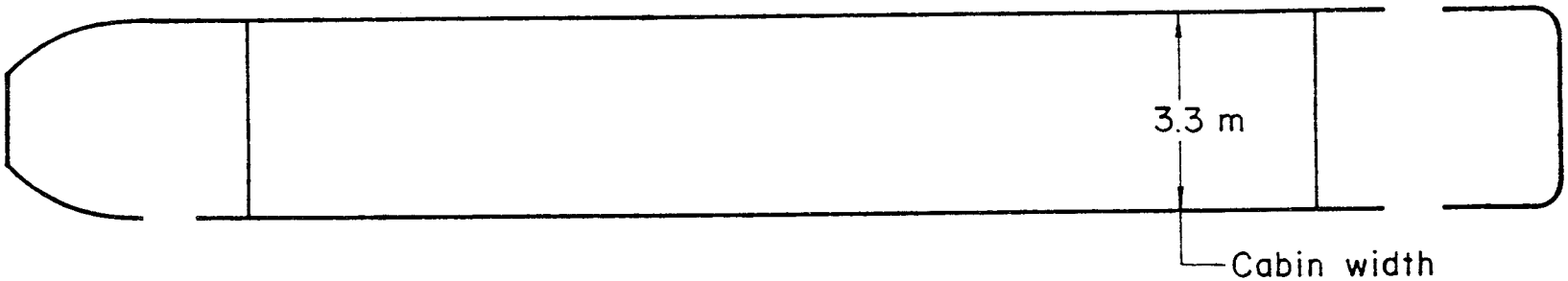

(b) PLAN AT CABIN FLOOR

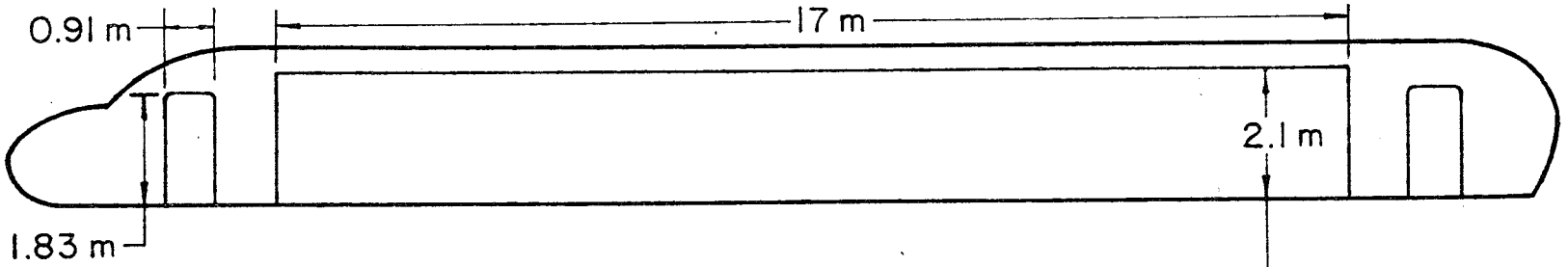

(a) ELEVATION AT MAXIMUM CABIN HEIGHT

Figure 1 737 Test Cabin Geometry

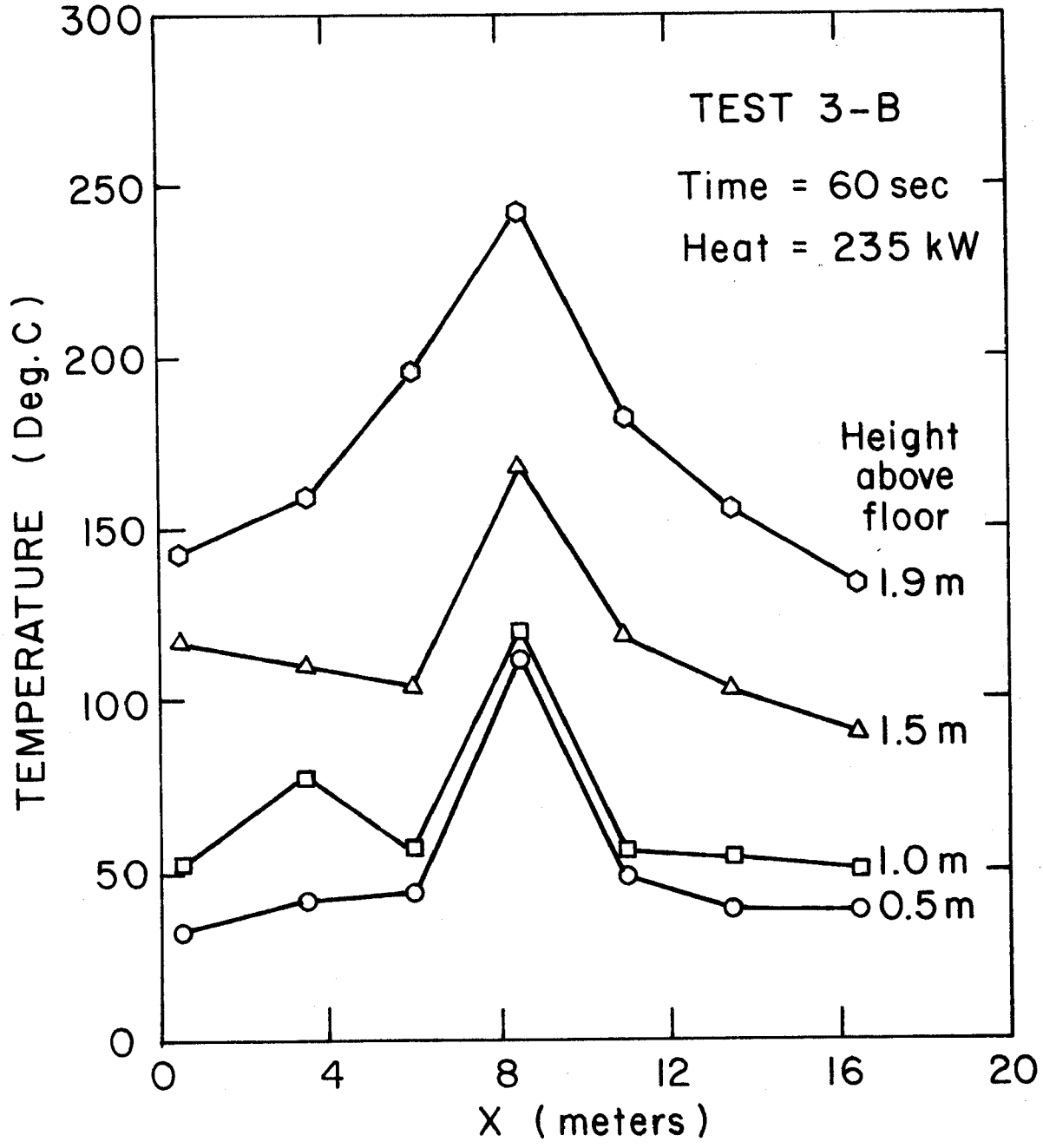

Figure 2 Experimental Temperature Profile

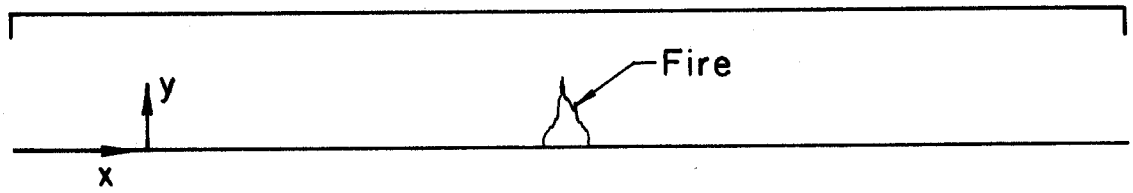

Figure 3 Simulated Test Cabin Geometry

$$\bar{x} = \frac{x}{H} \quad , \quad \bar{y} = \frac{y}{H} \quad , \quad \bar{t} = \frac{U_o t}{H} \quad ,$$

$$\bar{u} = \frac{u}{U_o} \quad , \quad \bar{v} = \frac{v}{U_o} \quad , \quad \bar{T} = \frac{T}{T_o} \quad , \tag{1}$$

$$\bar{\rho} = \frac{\rho}{\rho_o} \quad , \quad \bar{\rho}_E = \frac{\rho_E}{\rho_o} \quad , \quad \bar{P} = \frac{P-P_E}{\rho_o U_o^2} \quad ,$$

where the subscripts 0 and E refer to reference quantities and the hydrostatic equilibrium condition, respectively. The meaning of the symbols is listed in the List of Symbols. The resulting governing equations may now be written as follows:

$$\bar{\rho}\bar{T} = \frac{U_o^2}{RT_o} \bar{P} + \bar{\rho}_E \bar{T} \tag{2}$$

$$\frac{\partial \bar{\rho}}{\partial t} + \frac{\partial}{\partial \bar{x}} (\bar{\rho}\ \bar{u}) + \frac{\partial}{\partial \bar{y}} (\bar{\rho}\ v) = 0 \tag{3}$$

$$\frac{\partial}{\partial \bar{t}} (\bar{\rho}\ \bar{u}) + \frac{\partial}{\partial \bar{x}} (\bar{\rho}\ \bar{u}^2) + \frac{\partial}{\partial \bar{y}} (\bar{\rho}\ \bar{u}\ \bar{v}) = - \frac{\partial P}{\partial \bar{x}} + \frac{\partial \bar{\tau}_{xx}}{\partial \bar{x}} + \frac{\partial \bar{\tau}_{xy}}{\partial \bar{y}} \tag{4}$$

$$\frac{\partial}{\partial \bar{t}} (\bar{\rho}\ \bar{v}) + \frac{\partial}{\partial \bar{x}} (\bar{\rho}\ \bar{u}\ \bar{v}) + \frac{\partial}{\partial \bar{y}} (\rho\ \bar{v}^2) = - \frac{\partial P}{\partial \bar{y}} - \frac{gH}{U_o^2} (\bar{\rho}-\bar{\rho}_E) + \frac{\partial \bar{\tau}_{xy}}{\partial \bar{x}} + \frac{\partial \bar{\tau}_{yy}}{\partial \bar{y}} \tag{5}$$

$$\frac{\partial}{\partial \bar{t}} (\bar{\rho}\ \bar{T}) + \frac{\partial}{\partial \bar{x}} (\bar{\rho}\ \bar{u}\ \bar{T}) + \frac{\partial}{\partial \bar{y}} (\bar{\rho}\ \bar{v}\ \bar{T}) = \nabla \cdot (\frac{1}{Re_t Pr_t} \nabla \bar{T}) \tag{6}$$

where g is the gravitation constant and

$$\bar{\tau}_{xx} = \frac{2}{Re_t} \frac{\partial \bar{u}}{\partial \bar{x}} \quad , \quad \bar{\tau}_{xy} = \frac{1}{Re_t} (\frac{\partial \bar{u}}{\partial \bar{y}} + \frac{\partial \bar{v}}{\partial \bar{x}}) \quad , \quad \bar{\tau}_{yy} = \frac{2}{Re_t} \frac{\partial \bar{v}}{\partial \bar{y}} \quad , \tag{7}$$

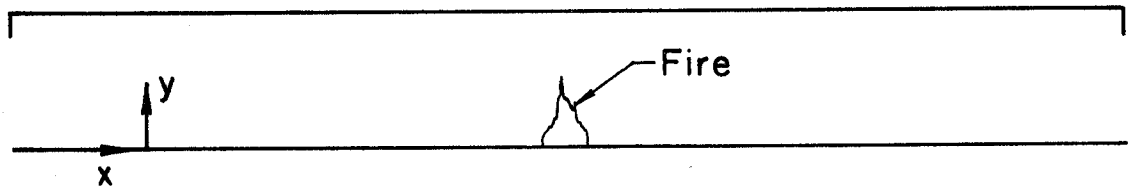

Figure 3 Simulated Test Cabin Geometry

and

$$Re_t = \frac{\rho_o U_o H}{\mu_{eff}} \quad , \quad Pr_t = \frac{\mu_{eff} C_{po}}{k_{eff}}$$

where the subscript "eff" on viscosity and conductivity stands for effective (laminar plus turbulent) transport.

In the present study, an algebraic turbulence model for recirculating buoyant flows with large variations in the turbulence level is employed[7]. In dimensionless form it may be written as

$$\frac{\mu_{eff}}{\mu_o} = 1 + \frac{\left[\left(\frac{\partial \bar{u}}{\partial \bar{y}}\right)^2 + \left(\frac{\partial \bar{v}}{\partial \bar{x}}\right)^2\right]^{1/2} \left(\frac{\ell}{H}\right)}{2 + \frac{Ri}{Pr_{tb}}} \tag{8}$$

where μ_o is the reference molecular viscosity and ℓ is the mixing length given by

$$\frac{\ell}{H} = K \left\{ \frac{(\bar{u}^2 + \bar{v}^2)^{1/2}}{\left[\left(\frac{\partial \bar{u}}{\partial \bar{x}}\right)^2 + \left(\frac{\partial \bar{u}}{\partial \bar{y}}\right)^2 + \left(\frac{\partial \bar{v}}{\partial \bar{x}}\right)^2 + \left(\frac{\partial \bar{v}}{\partial \bar{y}}\right)^2\right]^{1/2}} + \right.$$

$$\left. \frac{\left[\left(\frac{\partial \bar{u}}{\partial \bar{x}}\right)^2 + \left(\frac{\partial \bar{u}}{\partial \bar{y}}\right)^2 + \left(\frac{\partial \bar{v}}{\partial \bar{x}}\right)^2 + \left(\frac{\partial \bar{v}}{\partial \bar{y}}\right)^2\right]^{1/2}}{\left[\left(\frac{\partial^2 \bar{u}}{\partial \bar{x}^2}\right)^2 + \left(\frac{\partial^2 \bar{u}}{\partial \bar{y}^2}\right)^2 + \left(\frac{\partial^2 \bar{v}}{\partial \bar{x}^2}\right)^2 + \left(\frac{\partial^2 \bar{v}}{\partial \bar{y}^2}\right)^2\right]^{1/2}} \right\} \tag{9}$$

where K is an adjustable constant. Ri is the gradient Richardson number given by

$$Ri = \frac{Hg \left(\frac{\partial \bar{T}}{\partial \bar{y}}\right)}{U_o^2 \left(\frac{\partial \bar{u}}{\partial \bar{y}}\right)^2} \tag{10}$$

The effective conductivity k_{eff} is related to the effective vicosity μ_{eff} by the following expression

$$\frac{k_{eff}}{\mu_o Cp_o} = \frac{1}{Pr} + \frac{1}{Pr_{tb}} \left[\frac{\mu_{eff}}{\mu_o}\right] \tag{11}$$

The turbulent Prandtl number Pr_{tb} is taken to be unity in this study.

The formulation of the finite-difference equations is based on the micro-control volume scheme introduced by Patankar and Spalding [8]. Details are given in reference 1 for uniform rectangular cells. Cells are so chosen that their boundaries coincide with physical boundaries for easy treatment of the boundary conditions. The resulting finite-difference equations can be represented in the general form:

$$- A_S\Phi_S - A_W\Phi_W + A_P\Phi_P - A_E\Phi_E - A_N\Phi_N = S_P \tag{12}$$

where Φ represents any dependent variable. Subscripts S, W, E, N inidicate the neighboring cells or node points and P is the point under consideration. In the implicit method used here, all Φ values are unknown at the current time step, and must be solved for simultaneously from a penta-diagonal coefficient matrix containing A_S, A_W, A_P, A_E, and A_N. Because of the general difficulty involved in inverting a penta-diagonal matrix, an alternating-direction line-by-line sweeping method has been used. Detailed description is given in references 1 and 3. The equation of state, Equation (2), includes the dimensionless quantity U_o^2/RT_o, which makes the pressure term six orders of magnitude smaller than other terms in buoyant flow near atmospheric conditions. Pressure is, therefore, very weakly coupled with the equation of state and has little direct effect on the density and temperature. Doria [6] pointed out that if the equation of state was used to solve for the pressure and the continuity equation for the density, the procedure would fail. A modified correction scheme [3] has been used and the pressure is obtained through an iterative process involving both the momentum and energy equations to satisfy mass conservation to a desired tolerance.

A concise criterion for numerical stability is difficult to obtain. In the present study, the following criterion based on the differencing scheme with upward differencing for the convection term is used as a guideline for selecting the time step in the two-dimensional cases:

$$\Delta\bar{t} \leq \frac{1}{\frac{2}{Re_t}\left[\frac{1}{\Delta\bar{x}^2} + \frac{1}{\Delta\bar{y}^2}\right] + \frac{|\bar{u}|}{\Delta\bar{x}} + \frac{|\bar{v}|}{\Delta\bar{y}}} \tag{13}$$

in addition, the limiting Courant number

$$\frac{|\bar{u}|_{max}\,\Delta\bar{t}}{\Delta\bar{x}} \leq 1 \qquad (14)$$

is also accommodated as a check. In the upward differencing scheme used in the present study, numerical errors due to false diffusion can be expected at large cell Peclet numbers [9]. However, due to the relatively large effective thermal diffusivity values which also include the turbulent contribution, the cell Peclet number encountered is still quite reasonable, and hence the effect of false diffusion is not expected to be serious.

NUMERICAL SIMULATION OF THE EXPERIMENTAL DATA

Altogether 27 numerical simulation runs have been carried out for a variety of the simulation parameters such as the heat source strength and distribution, the fire shape, the doorway height, and the level of turbulence in the test cabin for the purpose of comparing with the temperature data in Figure 2. Such a simulation is necessary, in view of the fact that the UNDSAFE code does not contain a combustion model at this time, and hence there is no a priori way to determine the specific volumetric heat source strength distribution and the shape of the fire or heat source. In addition, the mockup fire test deals with a three-dimensional cabin with three-dimensional effects concentrated essentially in the doorway region and immediately adjacent to the fire. Consequently, the doorway height must be somewhat adjusted to localize these three-dimensional effects in the two-dimensional simulations. However, no attempt has been made to achieve a perfect agreement between the numerical results and the experimental data, particularly in view of the various uncertainties in the experimental measurements. The primary objective of our comparisons is to demonstrate that the two-dimensional UNDSAFE code is capable of predicting the overall trends in gas dynamic and temperature behavior in the cabin as a result of a fire initiated on the floor of the test cabin and that the ranges of the various two-dimension geometrical and thermal loading parameters, which have a realistic correspondence to the real phenomenon, can be determined. A second objective is to demonstrate the sensitivity of the flow and temperature distributions to each of the test parameters so that the more important effects for the overall cabin phenomenon can be ascertained and future tests can be set up to obtain crucial data.

Out of the 27 computer runs, the best two-dimensional simulation is achieved with the specific parameters shown in Table 1. It is seen that the total heat load in the two-dimensional case is much higher than that of the actual test case. This is, however, expected in view of the fact that the actual burner is centrally located on the cabin floor, finite in both longitudinal and traverse directions, while the two-dimensional fire base is taken to be a long strip extending over the entire width of the cabin. The door height is seen to be lowered in the simulated case to conform to the three-dimensional effects close to the doorway. Of most interest are the simulated fire shape and the heat strength distribution within the fire envelope. It is seen here that a majority of the heat release in the fire occurs close to the top of the flame indicating that the fuel is not completely burned next to the floor. Also, the simulated flame height is about three times that of the fire base, and this conforms well to what is expected for this type of fire.

Table 1. DETERMINATION OF 2-D EQUIVALENT PARAMETERS

	EXPERIMENTS	2-D EQUIVALENT
Total Head Load	235 KW	349 KW
Door Height	1.56	1.05

Fire Shape and
Heat Load Distribution

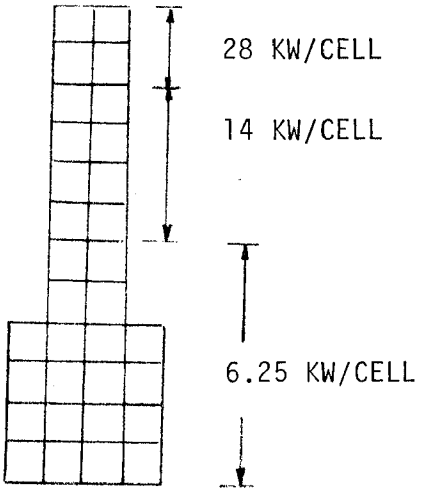

Constant K in Turbulence

Model 0.2

The comparison of the numerical results based on this test simulation case with the experimental data is shown in Figure 4. It is seen that the overall agreement is quite reasonable. The slight discrepancy in the temperature comparisons at the 1.5 meter height level can be remedied by further adjusting the local strength of the fire. This adjustment, however, is not done in view of the previously noted uncertainties in the measurements. The format in Figures 2 and 4 is that dictated by the thermocouple rake spacing used in the experimental program, and gives an erroneous impression of the actual temperature variations along the cabin length at a given height above the floor. This becomes clear when the detailed calculation results are plotted, as shown in Figure 5, where the width of the plume is much more realistically presented and is in general agreement with the existing plume literature.

Sensitivity studies have also been made relative to the various physical parameters and the results are shown in figures 6 to 9. Figure 6 shows the effect of strength of the fire source. It is seen that the strength primarily affects only the temperature level in the upper levels of the cabin, while the lengthwise temperature variation remains essentially unaffected. The effect of soffit height at the doorways is shown in Figure 7. The difference in the temperature levels is most pronounced at the height level of 1.0 meter. This is due to the presence of the larger door opening at that level for the case of 1.05 m of soffit height. The effect of varying the energy strength distribution within the fire shape is shown in Figure 8, in which the two-step distributions, relative to the fire shape as shown in Table 1, are given. It is found that the distribution of layers of hot gases is sensitive to variations of the local energy strength within the heat source envelope, namely the simulated flame. Finally, Figure 9 shows the effect of the turbulence level, particularly on the temperature behavior in the regions away from the fire source. Higher levels of turbulent viscosity implies higher degrees of mixing, and consequently the whole cabin enclosure is involved in both momentum and energy transfer at an earlier time after the fire initiation. As a result, the doorways will make their presence felt also at an earlier time for higher turbulence levels.

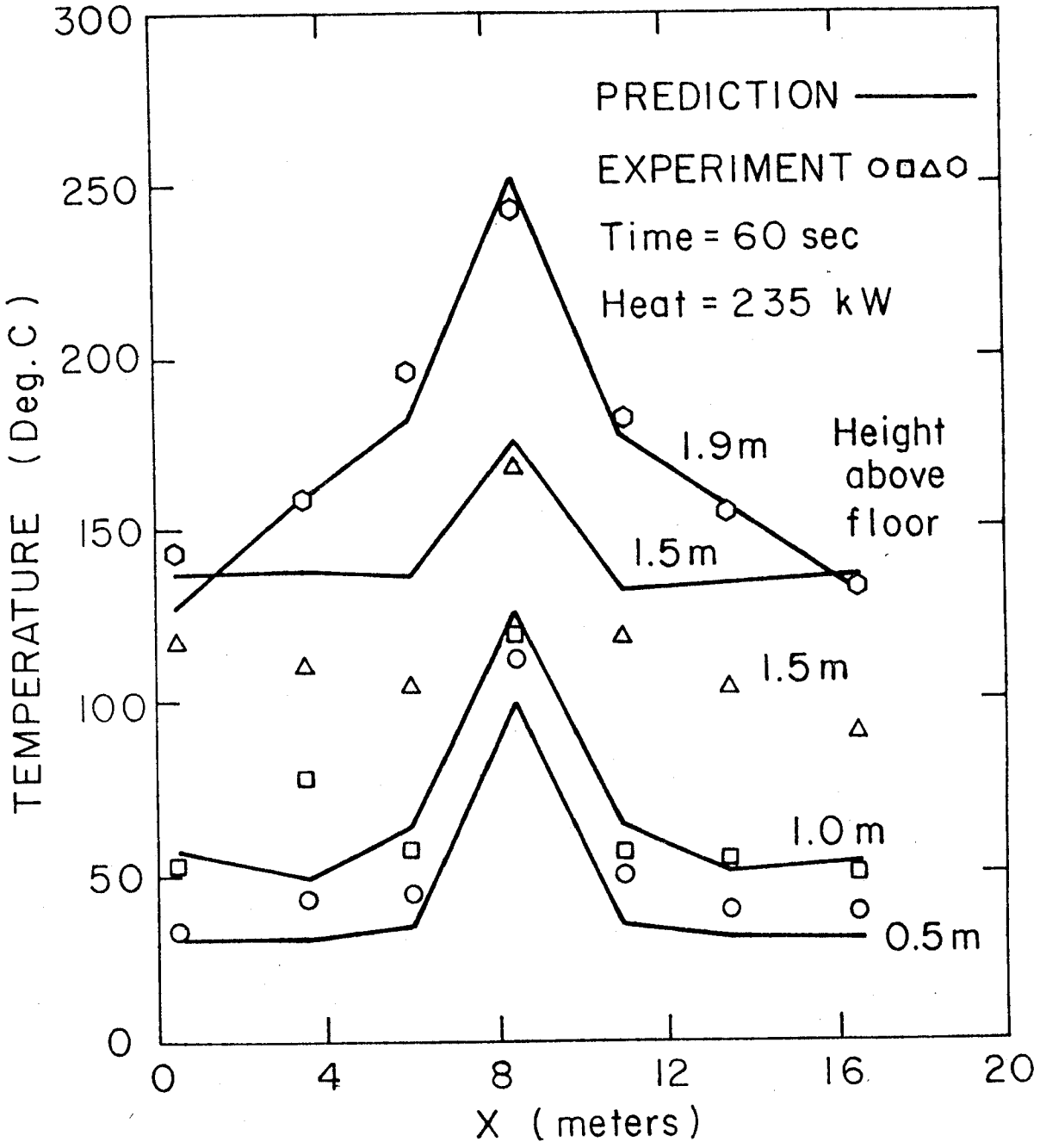

Figure 4 Comparison of Experiment with UNDSAFE Prediction

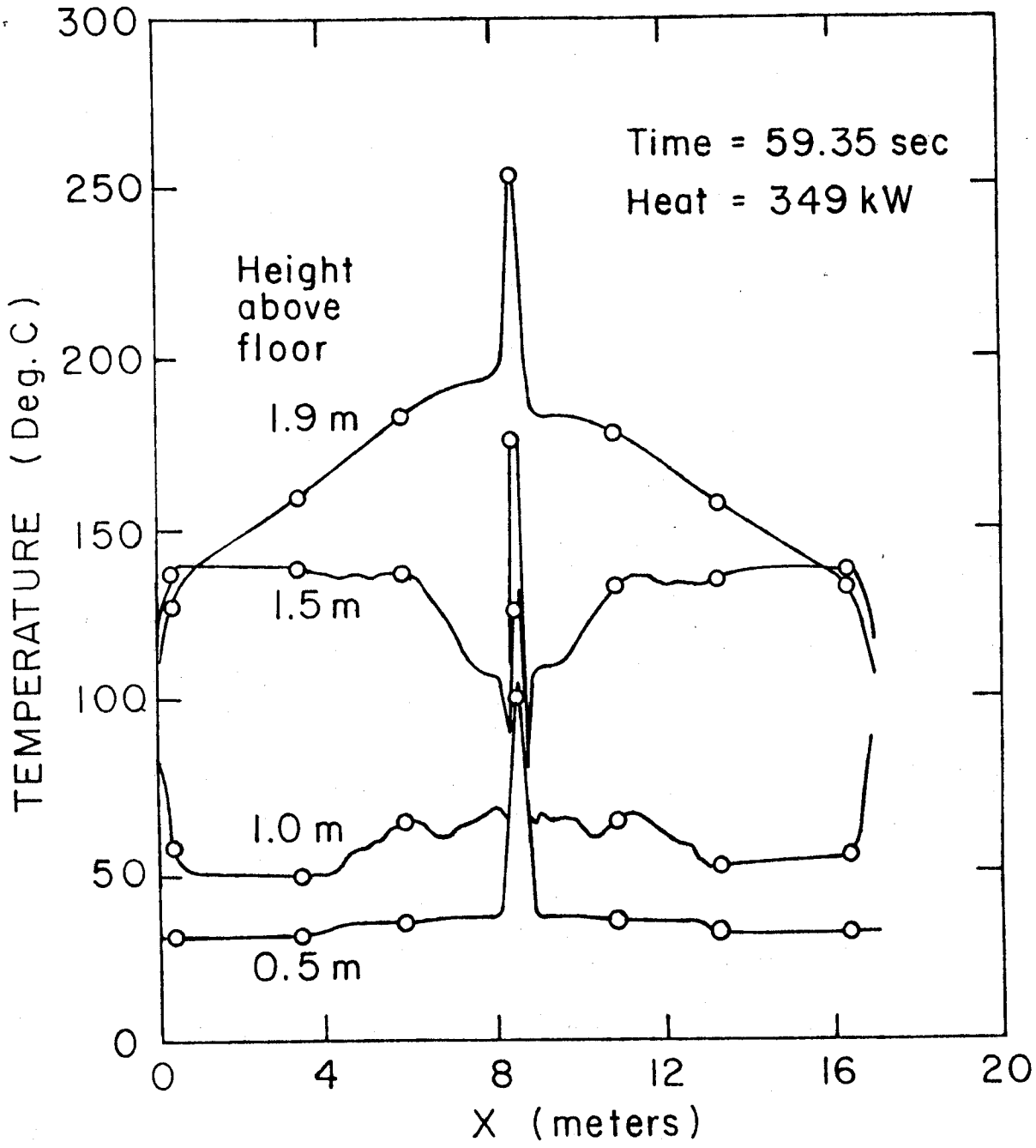

Figure 5 Importance of Rake-Spacing

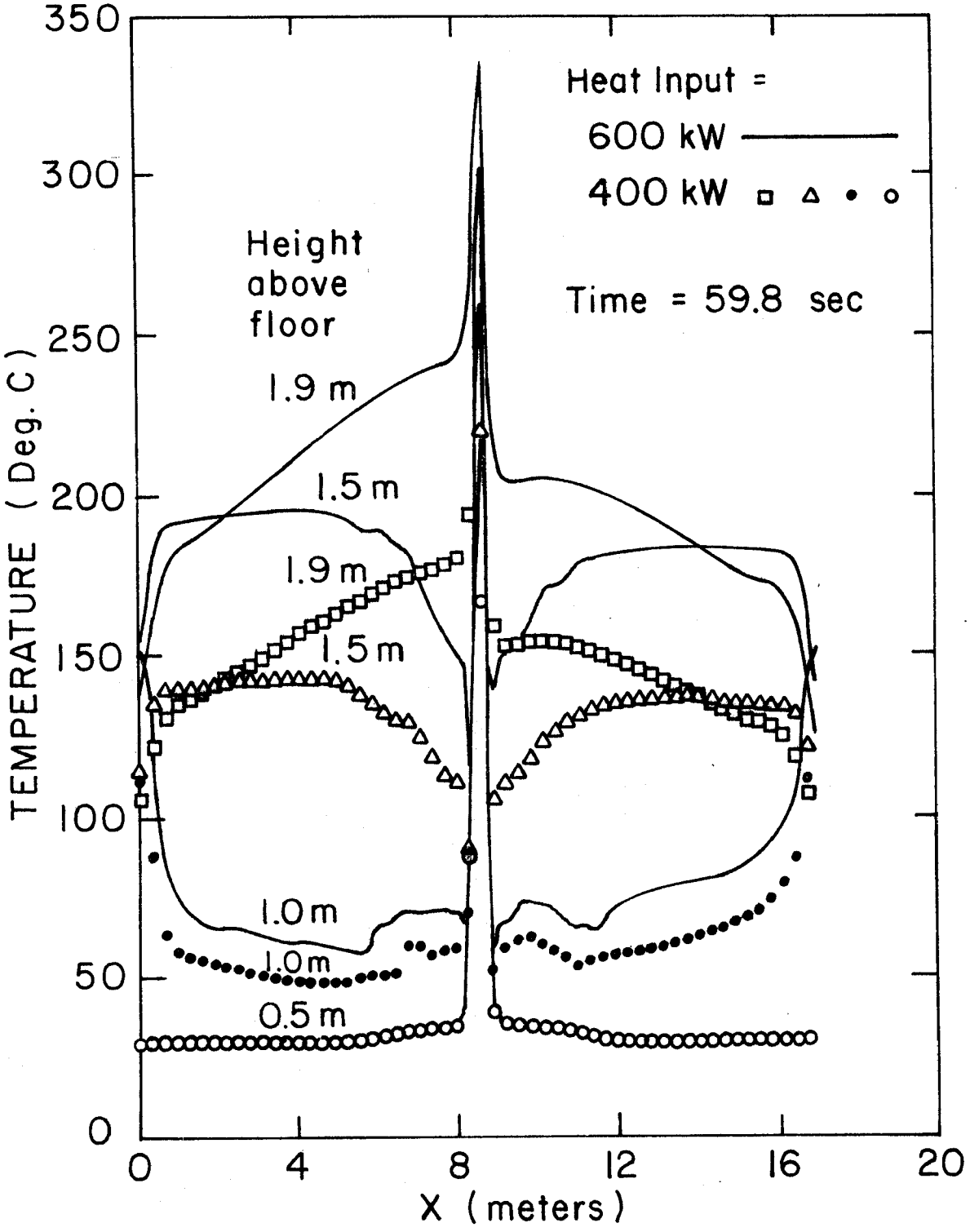

Figure 6 Effect of Heat Input Rate

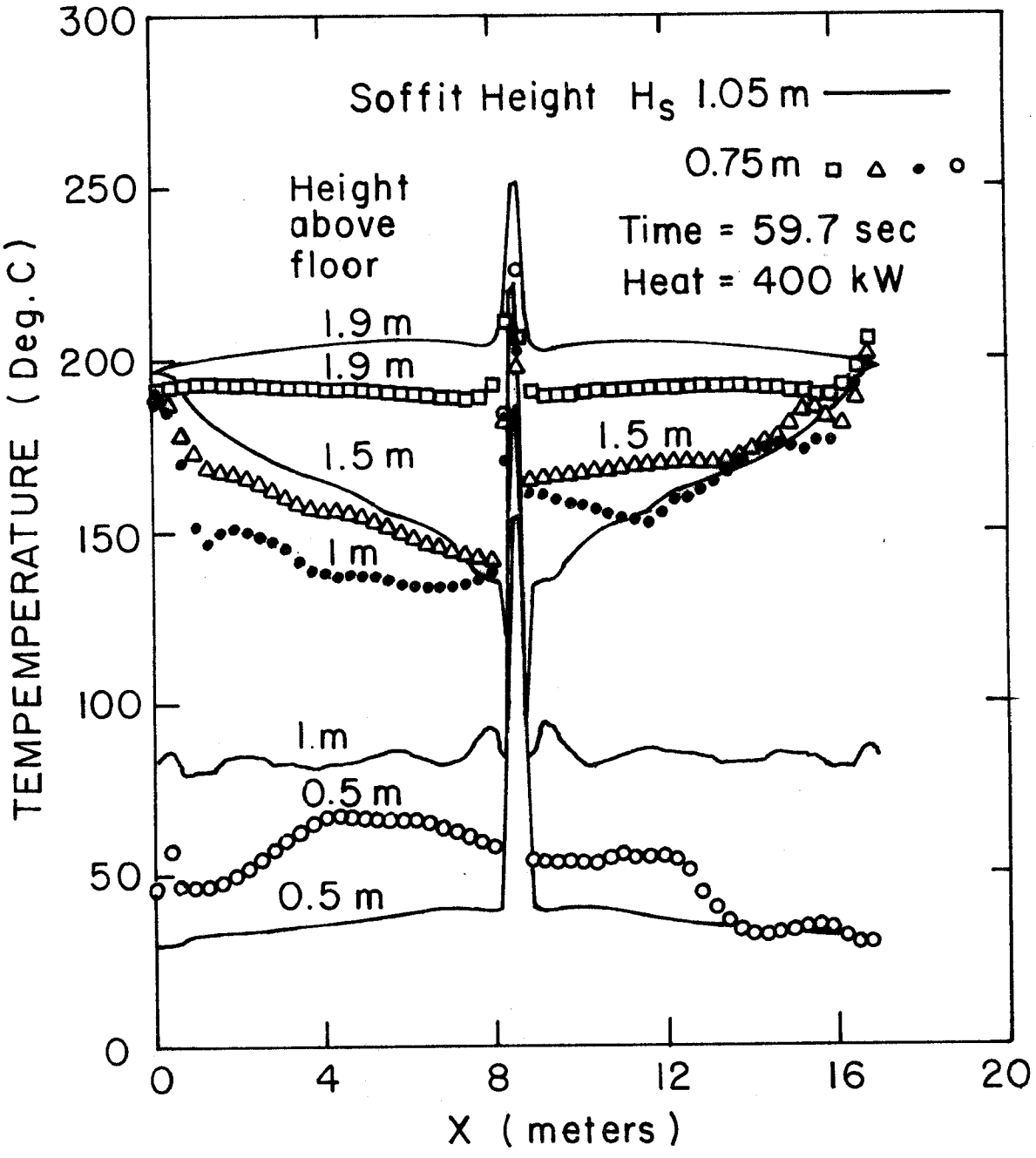

Figure 7 Effect of Soffit Height H_S

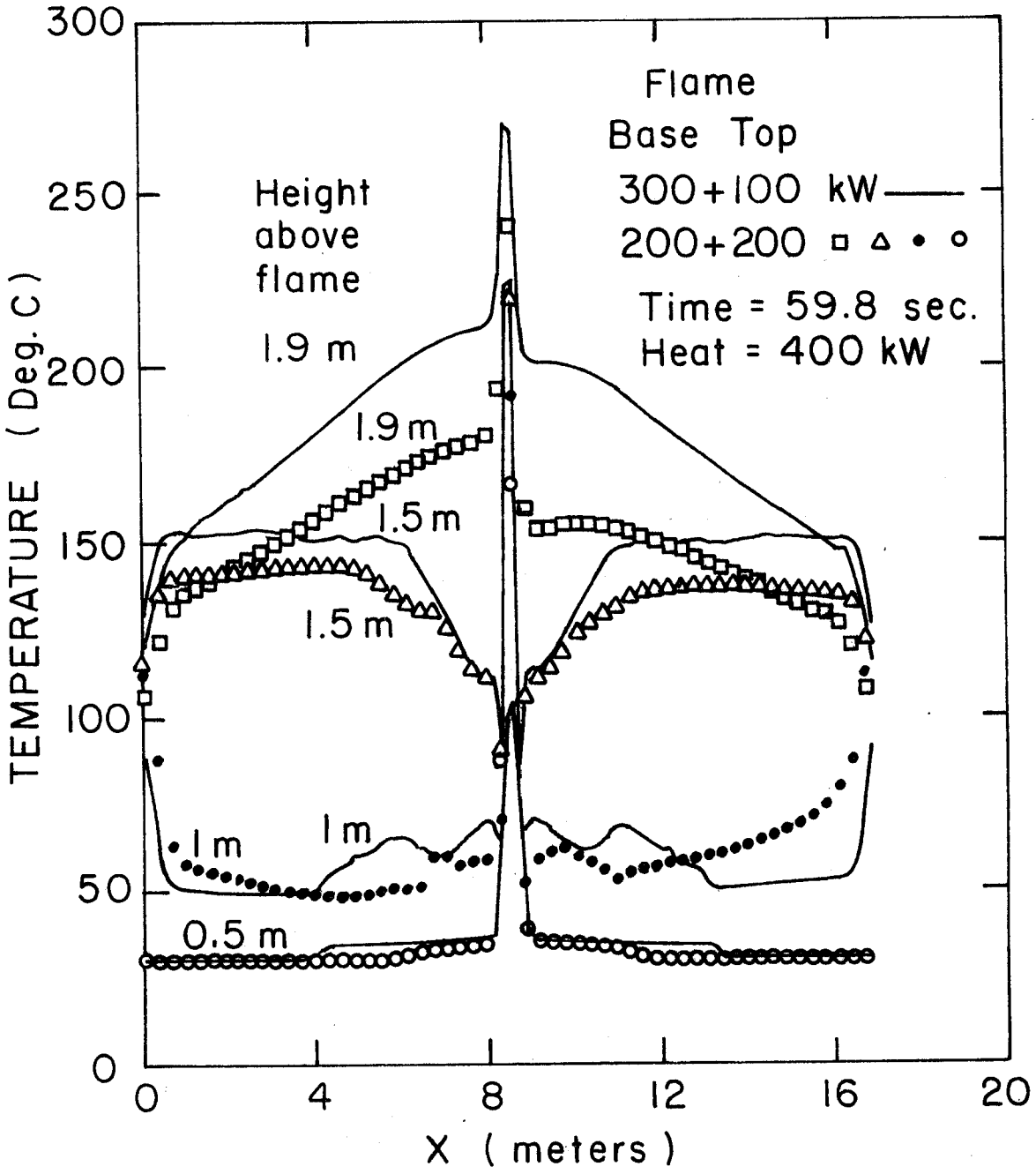

Figure 8 Effect of Energy Strength Distribution

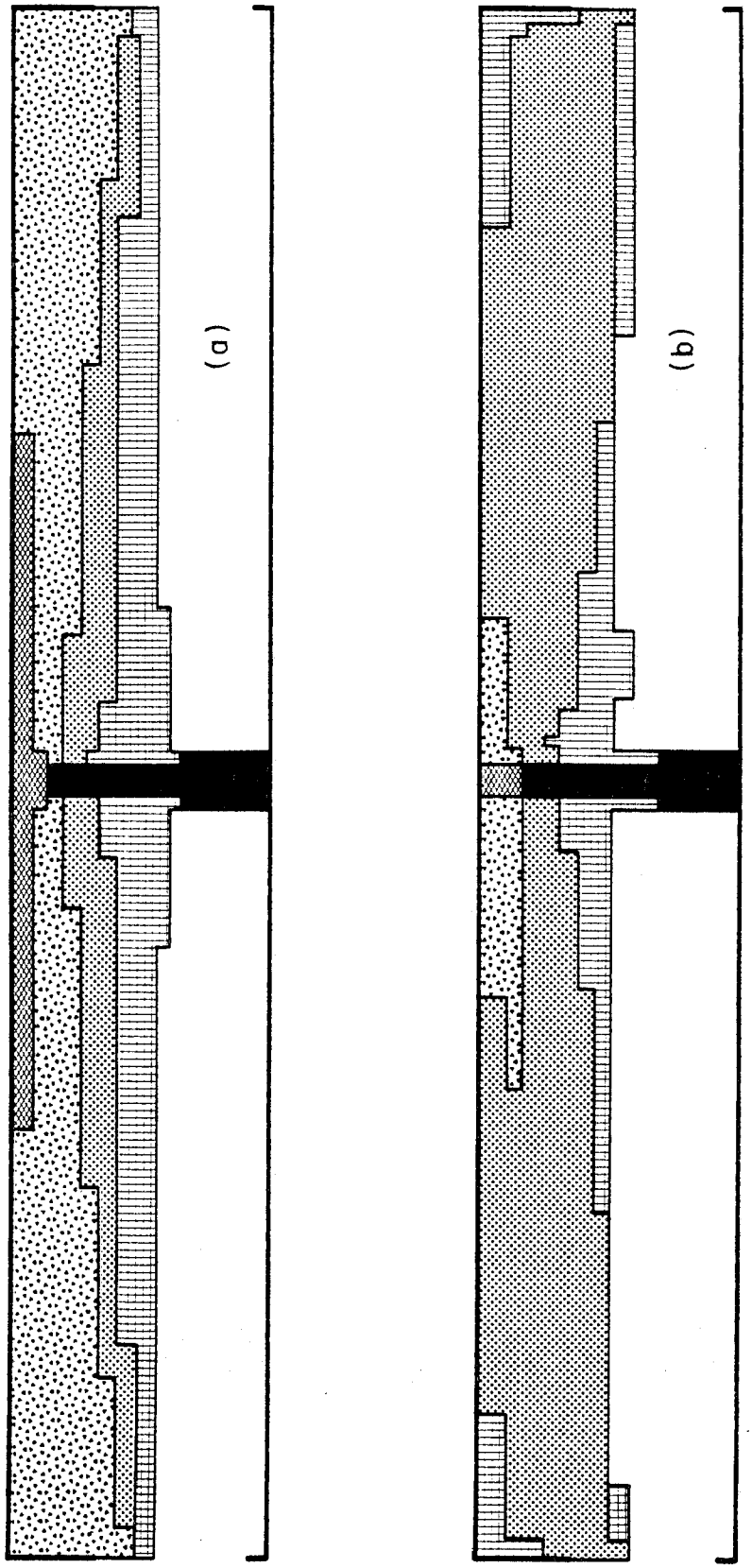

Figure 9 Effects of Turbulence Level

COMPUTER SIMULATION OF FIRES IN AIRCRAFT CABINS WITH SEATS

UNDSAFE CODE MODIFICATION

The simulation study of test 3-B in the cabin mockup fire test series conducted at the Johnson Space Center[4] has given us confidence in the ability to simulate realistic fire scenarios in aircraft cabins by means of the existing two-dimensional UNDSAFE computer code. It is now utilized to simulate the even more realistic situation of aircraft cabins with seats. Three additional modifications to the basic UNDSAFE code have been made for this simulation study as briefly presented below.

The presence of seats in the aircraft cabin dictates the modification of the basic UNDSAFE computer code to accommodate the new geometry in the computational field. A schematic diagram of this geometry is shown in Figure 10, which simulates a section of a typical wide-body aircraft cabin with six rows of high-back seats. The cabin front has a doorway and the cabin rear has a window or opening. The length of the cabin is established at 7.9 meters (26 feet) and all the other dimensions shown are in scale relative to the cabin length. Three different seating arrangements have been studied with the modified computer code: no seats, solid seats reaching the floow, and seats with opening at the floor. The case of no seats is chosen to simulate the condition along the open aisle in the aircraft cabin.

When seats are present in the cabin and fire is initiated close to these seats, there is a high probability that the seat surface temperature may become large enough to result in ignition so that additional heat may be added to the cabin fire flow. To accommodate such a scenario, the UNDSAFE code has been further modified to allow for additional heat generation when any surface cell of the seats reaches a prescribed temperature level. The strength of this addition can also be prescribed.

The final modification of the basic code is the incorporation of an additional equation which deals with the transport of smoke inside the aircraft cabin. It is assumed that there is no smoke generation inside the cabin except in the fire where the smoke generation rate is taken to be a prescribed constant. The governing equation for the smoke concentration Y can be written as

$$\frac{\partial}{\partial \bar{t}}(\bar{\rho}Y) + \frac{\partial}{\partial \bar{x}}(\bar{\rho}\bar{u}Y) + \frac{\partial}{\partial \bar{y}}(\bar{\rho}\bar{v}Y) = \nabla \cdot \left(\frac{1}{Re_t Sc_t}\nabla Y\right) \qquad (15)$$

where $Sc_t = \mu_{eff}/(\rho D_{eff})$ and D_{eff} is the effective diffusion coefficient. It is here seen that the smoke transport is governed by the balance between accumulation, convection, and diffusion. Boundary conditions are that smoke particle deposition at solid surface is negligible and that natural conditions are used at the doorway and the opening. A similar smoke transport has been considered in an earlier numerical study on compartment fires [10].

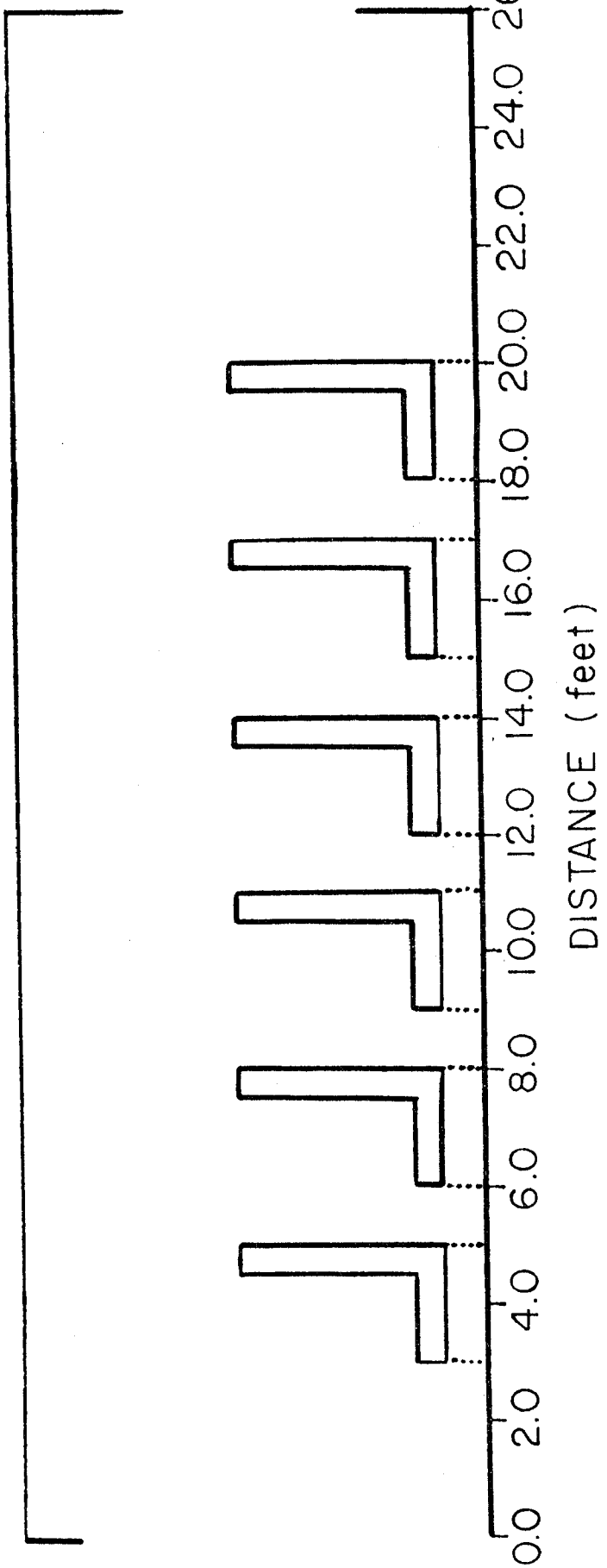

Figure 10 Simulated Wide-Body Aircraft Cabin Geometry

COMPUTER SIMULATION AND DISCUSSION OF RESULTS

Six complete runs have been carried out on the computer until steady-state conditions are achieved. They deal with two different fire configurations. In one, designated as Case A, the fire in the form of a volumetric heat and smoke source is initiated between the third and fourth rows of seats. In the other configuration, designated as Case B, a simulated fire with a flame height approximately three times the fire base and a flame strength distribution similar to that of the preceding study is located between the doorway and the first row of seats. For each of the two fire scenarios, three computer runs have been carried out for the three seat configurations. Results of the calculations in terms of the steady-state solutions are shown in Figures 11-28. Their discussion follows.

CASE A: HEAT SOURCE BETWEEN SEAT

In this scenario, the simulated fire source is located between the third and fourth rows of seats, and the volumetric source there generates uniformly a total of 350 kW. When the heat surface cells reach a dimensionless temperature of 2.0 (a dimensionless temperature of 1.0 designates a reference temperature of 300° K), additional heat is generated at the rate of 2.5 kW per cell, with a possible total of 97.5 kW for all the seat surface cells in the heat source zone. Such a fire source level typically represents a fire which can be expected to occur as a result of our previous simulation studies. In addition, a uniformly-distributed smoke source with a total strength of 0.046 kg/sec in the heat source zone is utilized to simulate the smoke generation in the fire. This strength has been chosen so that the resulting volumetric smoke density is of the order of 10^{-6} to 10^{-4} throughout the cabin, the appropriate level for a "dirty" fire. A convective thermal boundary condition at the cabin ceiling with an outside coefficient of heat transfer of 112.5 W/m^2K is taken to represent realistically the ceiling heat loss phenomenon.

Calculations for three seating configurations, as mentioned previously, have been carried out. Figure 11 shows the steady-state velocity field for the open aisle case, while Figures 12 and 13 give the corresponding velocity fields for the seat row cases with and without open bottoms. Figure 11 shows a plume above the heat source and the ceiling jets away from the plume. While at the left side of the cabin a relatively strong inflow of ambient air, which extends about two-thirds of the height from the floor, is quite evident; both the ceiling and floor soffits cause a much more complicated flow field at the right side of the cabin. A four-layered structure, similar to that found in room fires, can be discerned in the upper portion of the cabin and a recirculation zone close to the right lower corner. As will be seen later, this flow behavior on the right gives rise to higher levels of smoke concentration. Figure 12 shows a very different flow field when solid seats are present. Here one finds a very strong recirculation zone within the fire source, which also spawns a plume above the fire, undoubtedly due to the strong buoyancy there. On the other hand, the shear induced recirculation flows in other regions between the seats are relatively weak, the extent likely depending on the height of the seat back. Another interesting feature is that there exists a large vortex behind the last seat row which reduces the effectiveness of the back window as a supplier of ambient air there. Also it is of interest to note that part of the incoming flow at the left doorway close to the floor does not feed itself into the fire region. This is due primarily to the presence of the first seat row which acts as a flow barrier. Figure 13 shows the

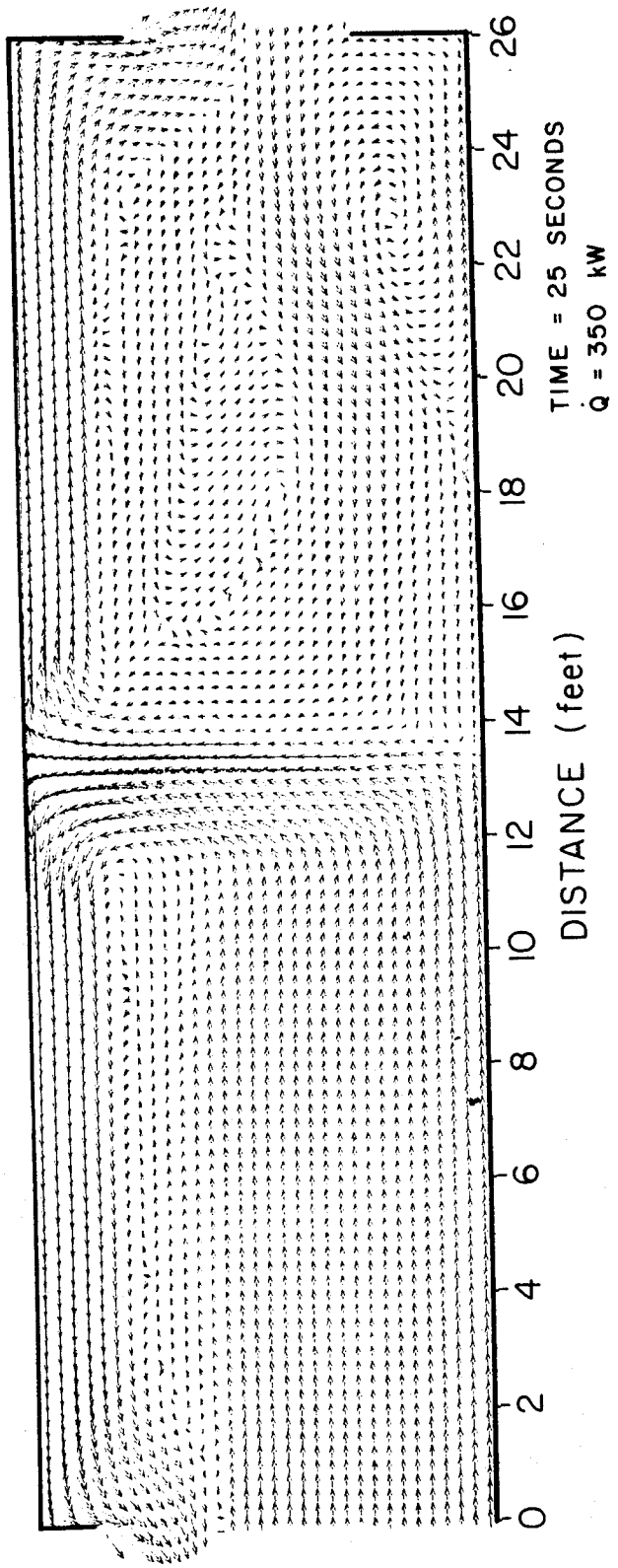

Figure 11 Velocity Field for Open Aisle, Case A

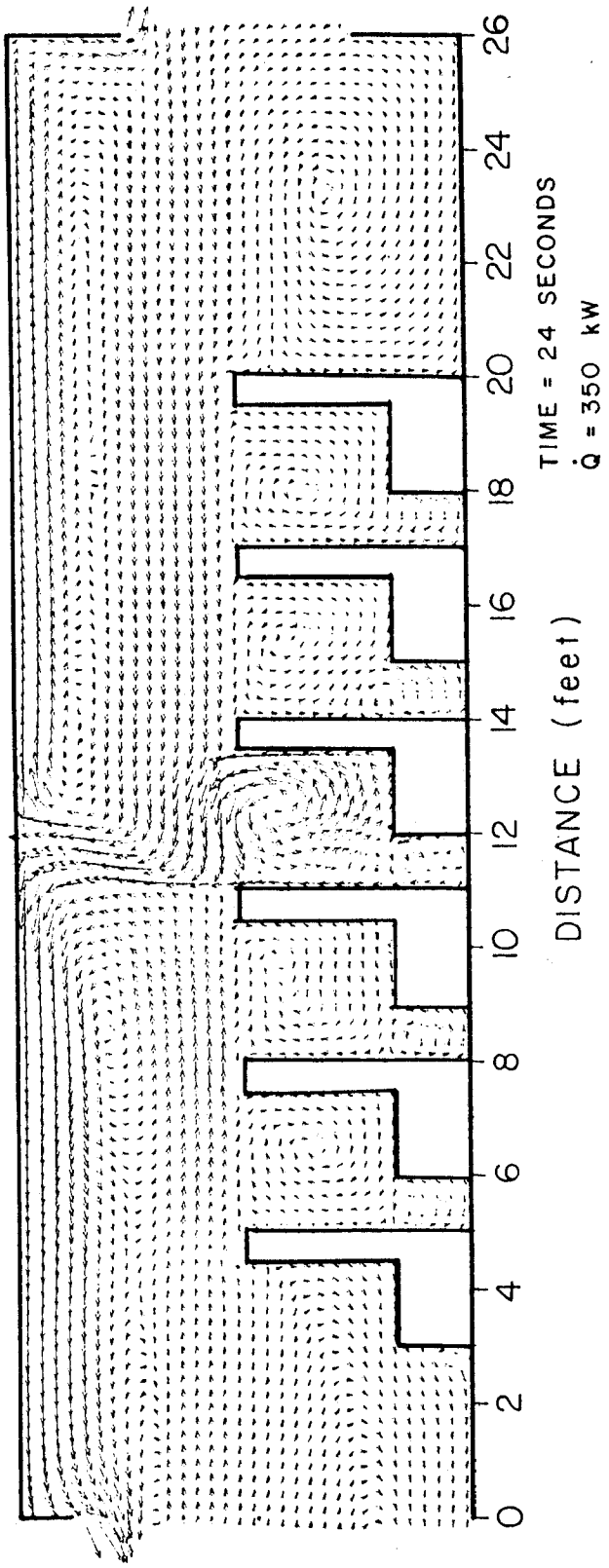

Figure 12 Velocity Field for Solid Seats, Case A

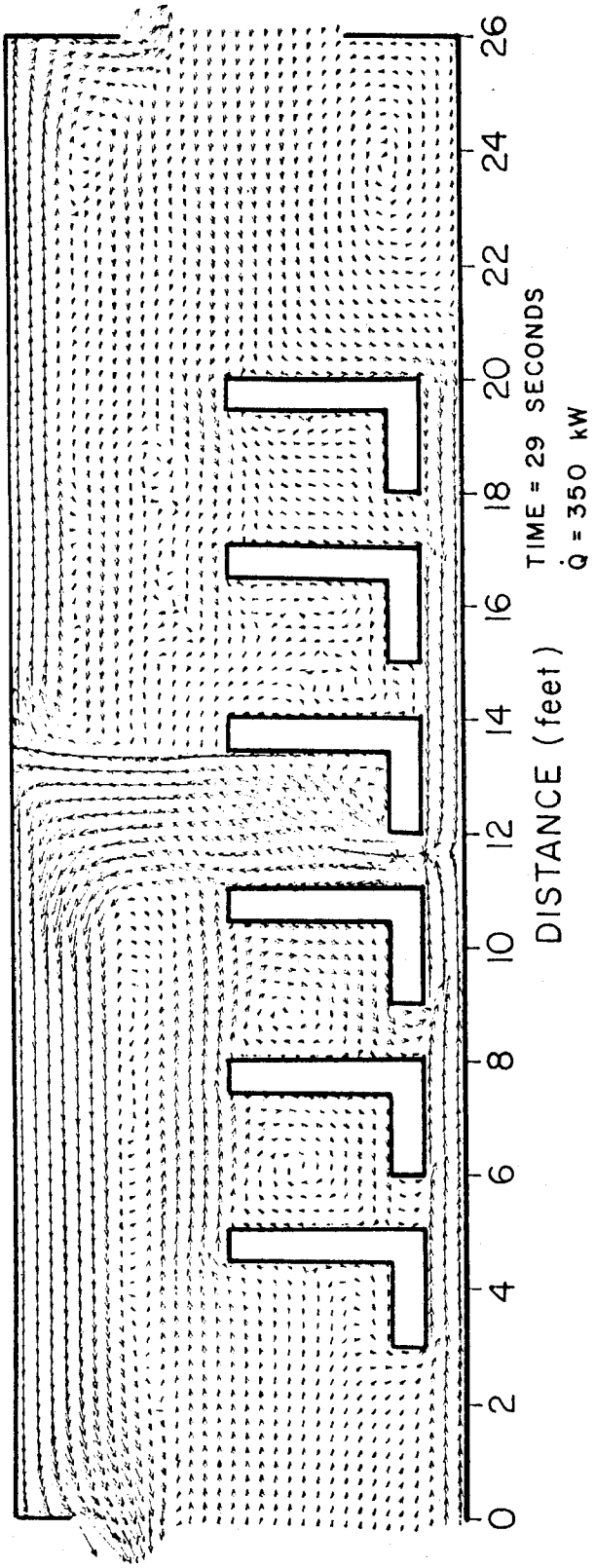

Figure 13 Velocity Fields for Open-Bottom Seats, Case A

corresponding flow field for the case of seats with open bottoms. The dominant feature here is the strong floor jets from both openings feeding into the fire plume. Of particular interest is the fact that the circulating flows between the seats also impart some of their mass to the floor jets. In this case, the large vortex in Figure 12 is greatly suppressed because of the seat bottom openings. Also, the stronger plume leaning to the left, due to the seat geometry, can be seen to give rise to a stronger ceiling jet.

The corresponding temperature fields and smoke-concentration fields are shown in Figures 14, 15, 16, 17, 18,, and 19, respectively. First of all, it may be noticed that these two sets of figures are quite similar in overall behaviors. This is primarily due to the fact that the governing differential equations are identical, and the associated boundary conditions are only slightly different. In the absence of thermal radiation, with constant properties, the two fields, properly normalized, should be identical, provided that the normalized boundary conditions are the same. For the sake of discussion, it is more interesting to examine the smoke-concentration plots in Figures 17, 18, and 19. For the open aisle case (Figure 17), much more smoke is present to the right of the fire due to the complex recirculating flow patterns in that region, as shown in Figure 11. Heavy smoke concentration can also be observed above the fire and along the ceiling. The region close to the floor to the left of the fire is essentially void of smoke in view of the strong inflow. In Figure 18, for the case of solid seats, heavy smoke is essentially confined to the ceiling region, and does not penetrate significantly into the seating area away from the fire zone. This behavior, as pointed out previously, is primarily due to the height of the seat back, and immediately suggests that for this type of seating, the seat-back height is an important parameter and should be as high as possible to prevent smoke penetration downward into the passenger seating area. A different situation, however, can be observed in Figure 19 for the case with open seat bottom. Because of the easier communication provided by the seat bottom openings, smoke penetration into the seating areas is much more severe, with the exception of the first seat rows. It is also seen that this situation is more severe in the areas to the right of the fire than to the left. This is primarily due to the presence of the bottom soffit at the right end of the cabin.

Further, Figures 15 and 16 also show an interesting result. In Figure 15 it is seen that the strong recirculating flow inside the fire zone (see Figure 12) causes all seat surface cells to reach the trigger temperature to release more heat. The plume-like flow in Figure 16, however, provides better ventilation so that only the right seat surface cells reach the trigger temperature, thus adding less additional heat into the flow field in the cabin.

CASE B: HEAT SOURCE IN THE CABIN FRONT

In order to see the effects of changing fire locations inside the cabin on the flow, temperature, and smoke-concentration fields, calculations have been made for the same three seating configurations but with the simulated fire source located midway between the left doorway and the first row of seats. In addition, a more realistic fire envelope shape and strength distribution obtained from our previous simulation studies were utilized. The total heat source strength remains essentially the same at 349 kW, but the total smoke generation rate is now 0.057 kg/sec with local smoke generation rate directly proportional to the local heat source strength.

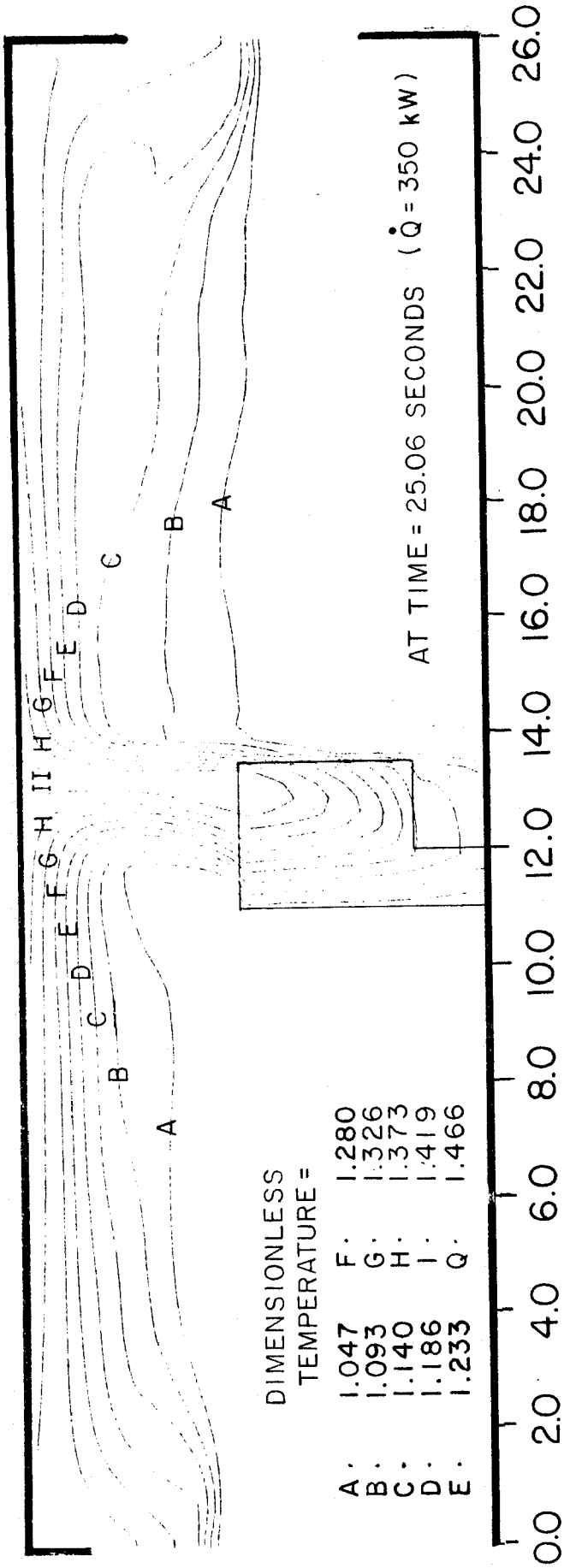

Figure 14 Isotherms for Open Aisle, Case A

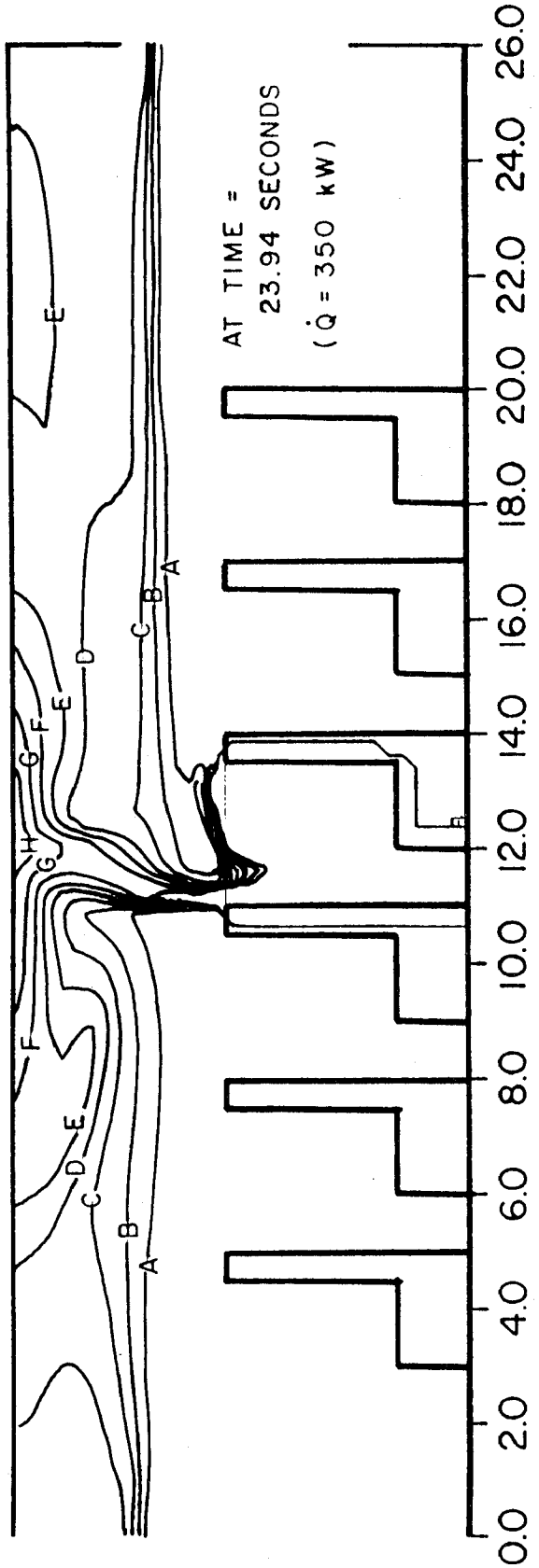

Figure 15 Isotherms for Solid Seats, Case A

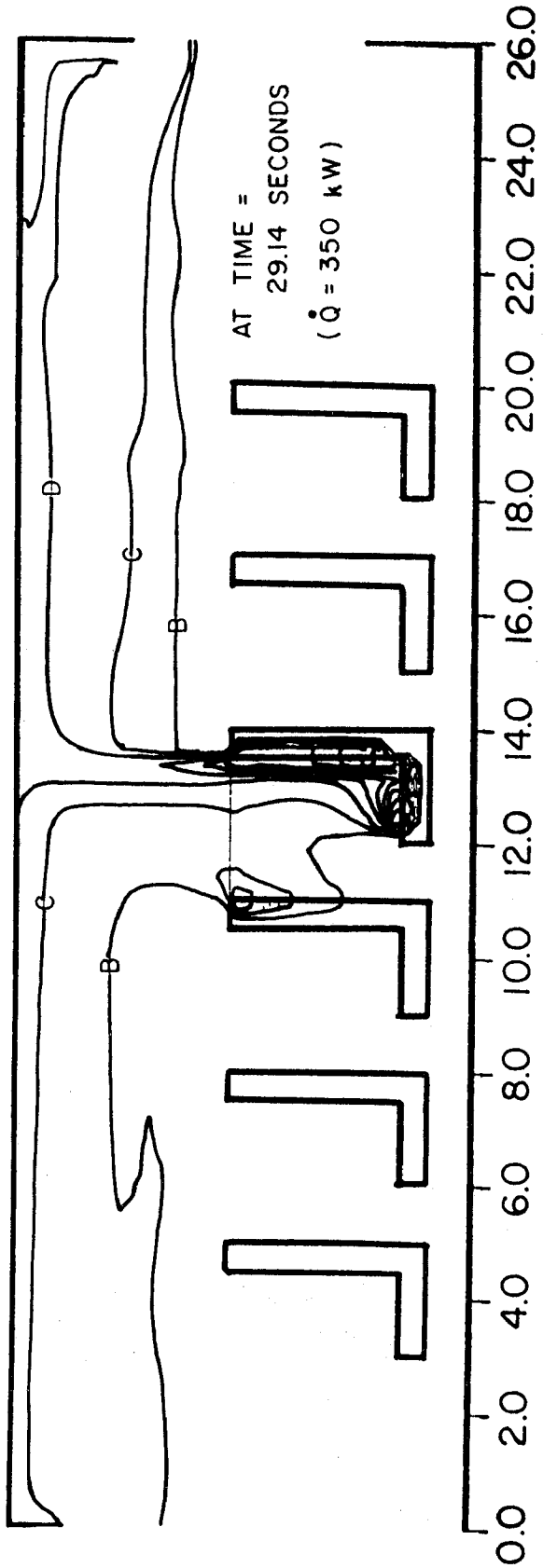

Figure 16 Isotherms for Open-Bottom Seats, Case A

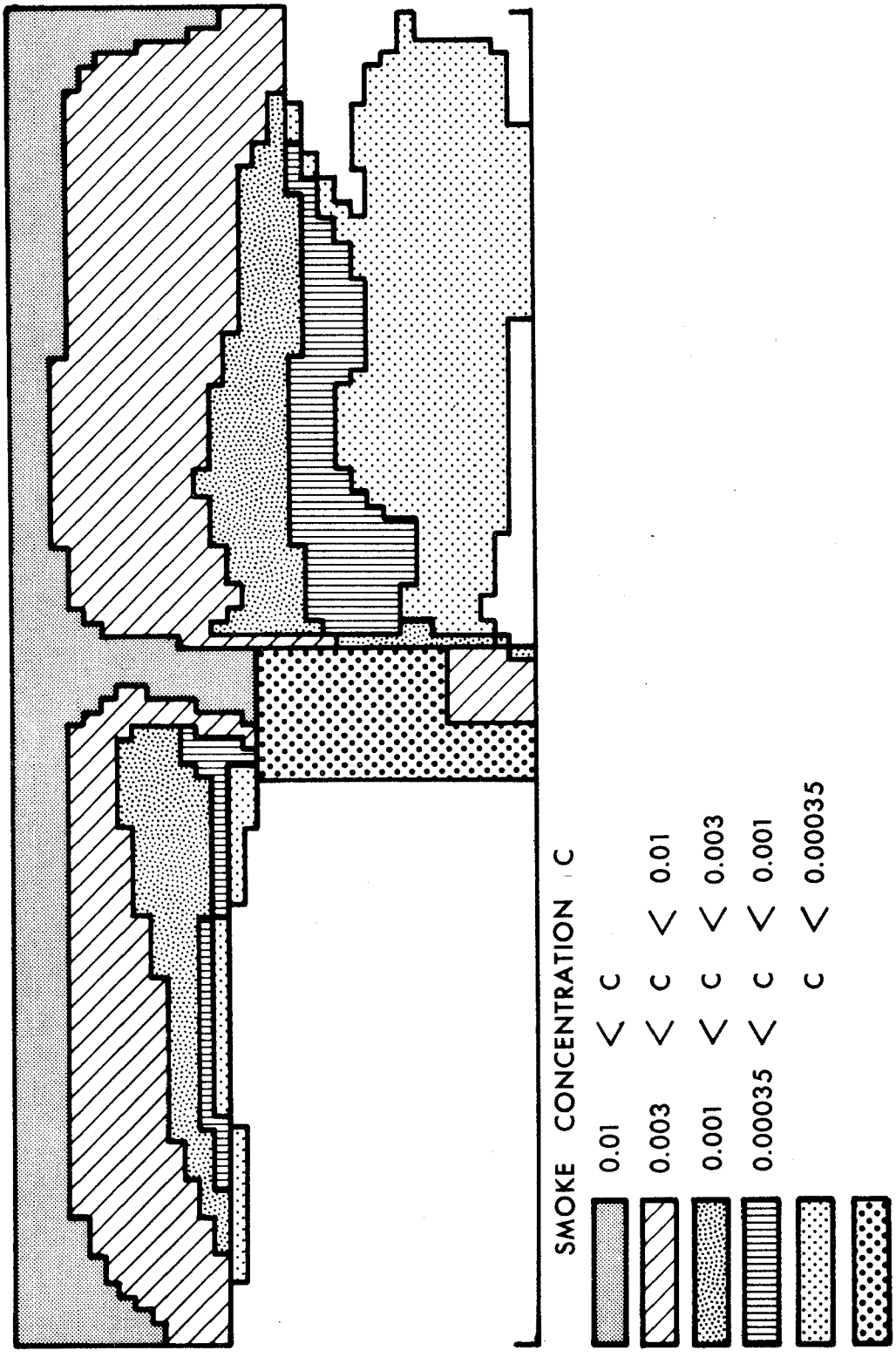

Figure 17 Smoke Distribution for Open Aisle, Case A

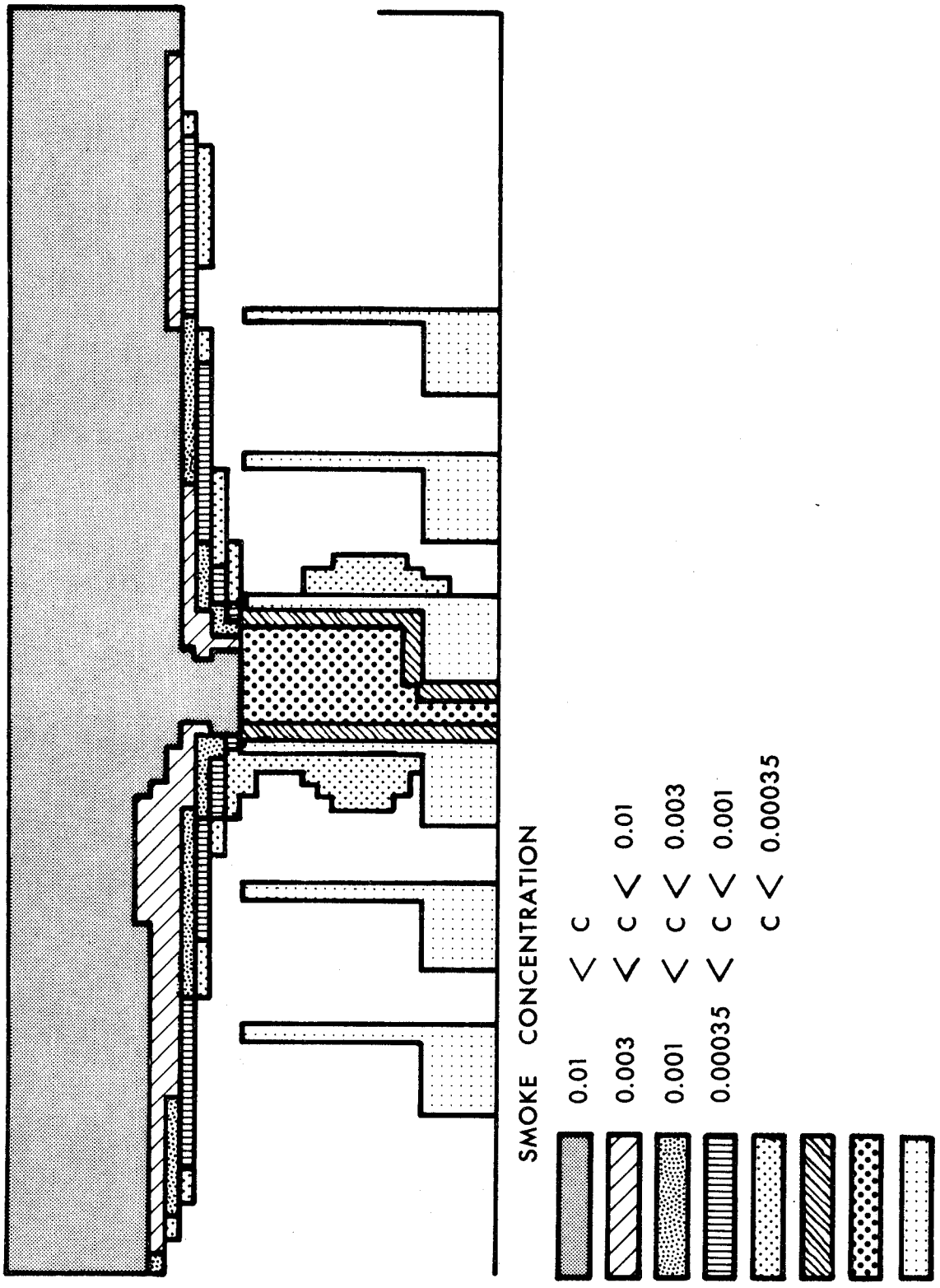

Figure 18 Smoke Distribution for Solid States, Case A

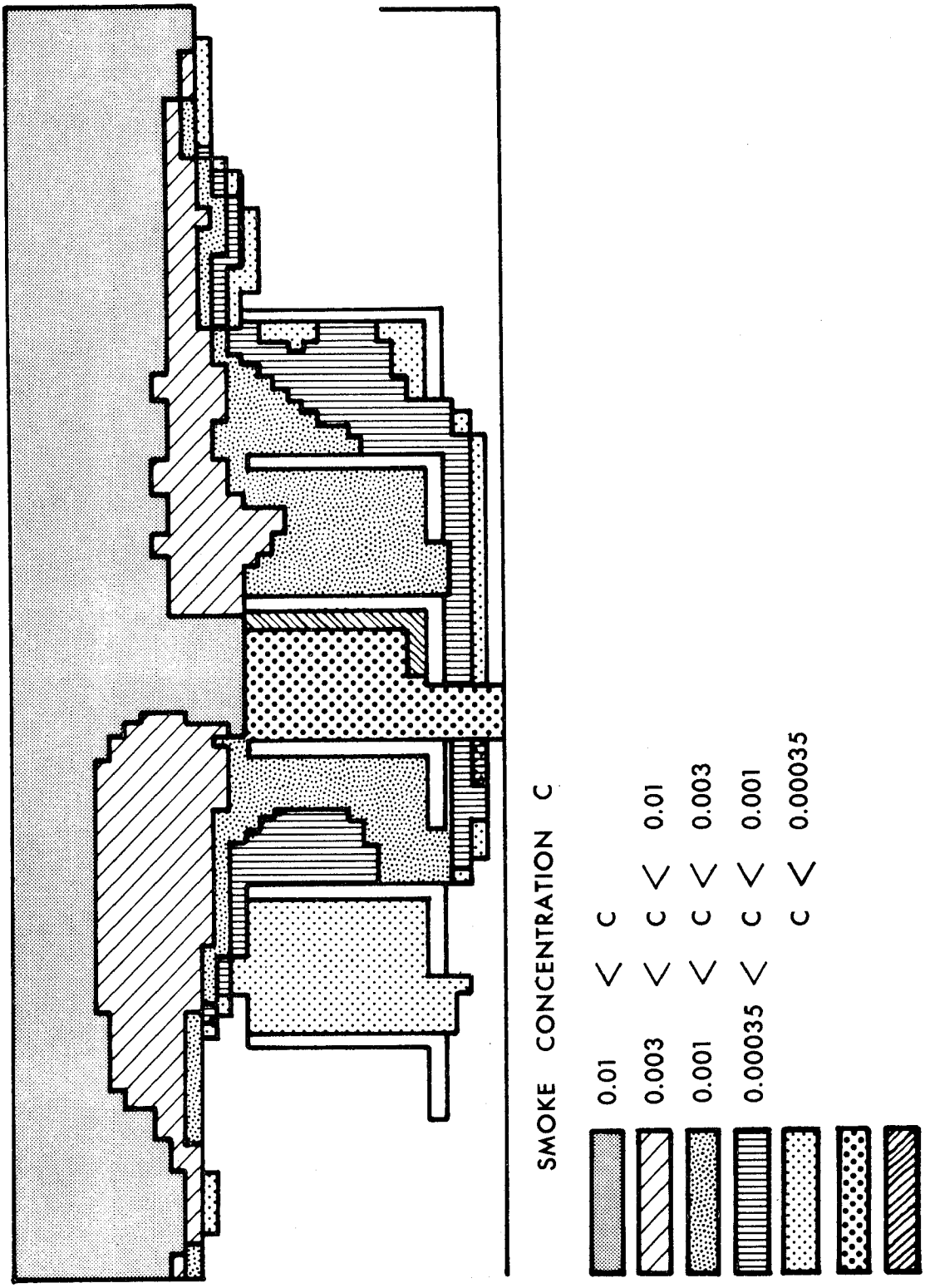

Figure 19 Smoke Distribution for Open-Bottom Seats, Case A

Three velocity fields are shown in Figures 20, 21, and 22. In Figure 20 for the open aisle case, the heat source acts very much like a thermal pump which basically draws the fluid from the doorway opening at the left and pushes the flow through the length of the cabin and out of the opening at the right. Local deviations from this basic behavior are prominent only in the region immediately to the right of the flame tip where the buoyancy effect is locally quite significant. While the basic feature remains the same for the case of the solid seats as shown in Figure 21, the effect of the presence of the solid seats is dramatic. A twin vortex system behind the last seat row can be seen. Also, the flow is reversed in the region immediately above the seats, which appears to be due to the obstruction provided by the ceiling soffit at the right end of the cabin. This reversed flow, which is not very strong, is also responsible for the vortex-type flows within the seating areas. It is also of interest to note the double vortex flow pattern in the region between the last two seat rows. The flow field is even more dramatically altered in the case of seats with an open bottom, as shown in Figure 22. The buoyancy-induced in-flow at the left is seen to be broken up into two main streams, one at the top and the other at the floor below the seats, which essentially recombine at the window exit at the right. The shear flow between these two streams is greatly altered by the presence of the seats and the soffits at the right end. The choking at the exit produces a reveresed flow which again interacts with the main streams in the vicinity of the seats. One very interesting phenomonen is that the vortex flow in the seating areas observed in Figure 21 are essentially washed away and no longer exist. Another very interesting feature of the flow field is that there exist plume-like flows, which are not of thermal nature, between the second and third seat rows and between the fourth and fifth seat rows. The left plume is sufficiently strong to reach vertically to join the main ceiling jet.

The temperature fields for the three seat configurations are shown in Figures 23, 24, and 25. For the open aisle, low temperatures are found throughout the cabin except in the immediate neighborhood of the fire tip where large temperature gradients occur. In the solid seat case (Figures 24), the ceiling layer becomes slightly warmer, and seating areas are essentially protected from heat, including the first seat rows. This is primarily due to the large cool in-flow from the doorway. However, it must be realized that in reality the first seat row is directly exposed to flame radiation and hence would become quite hot. In the present study, thermal radiation is not included. For the case of seats with open bottom, the heat penetration into the seating areas is slightly more severe (see Figure 25), while the ceiling jet also becomes slightly warmer. The corresponding smoke concentration fields are shown in Figures 26, 27, and 28. The severity due to smoke concentration is seen to follow very closely that due to heat. It may be concluded that when the fire is located close to the front doorway, the seating areas are quite effectively protected from both heat and smoke with possible exception of the first seat rows.

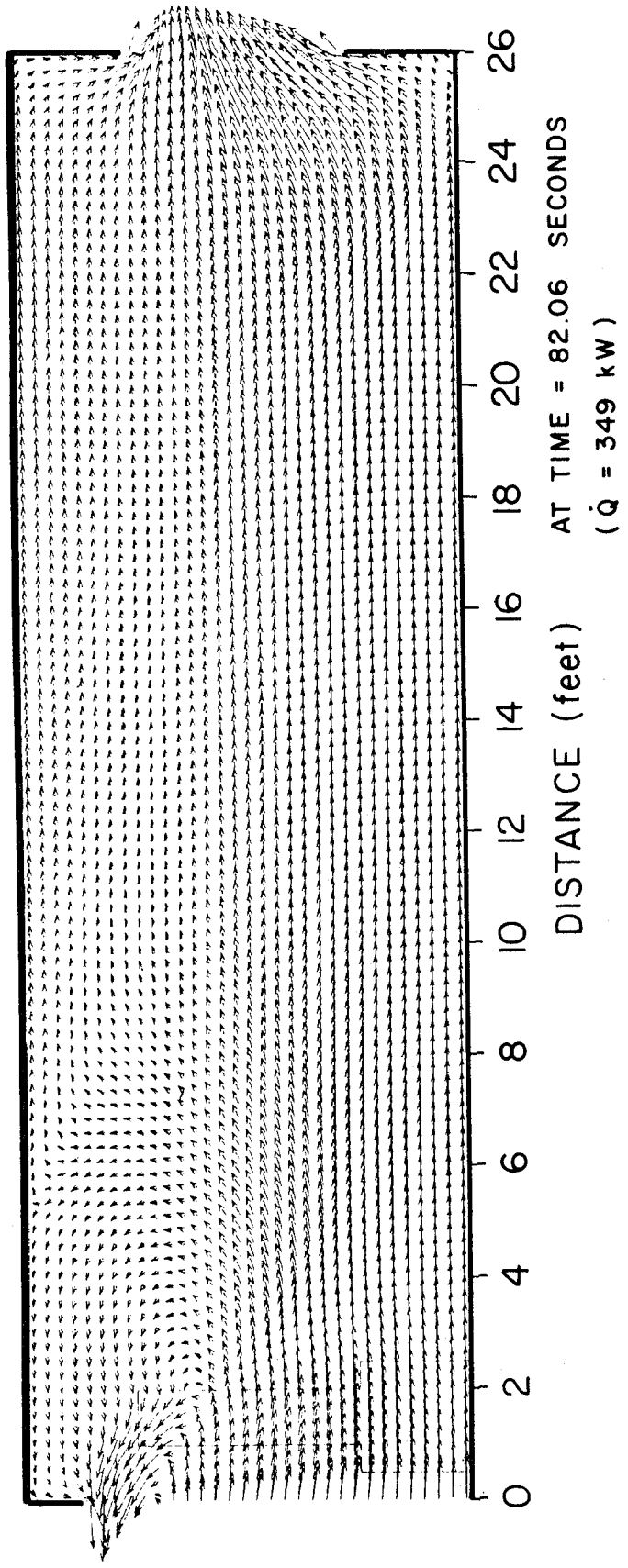

Figure 20 Velocity Field for Open Aisle, Case B